# Stabilization of Neurotoxic Soluble $\beta$-Sheet-Rich Conformations of the Alzheimer's Disease Amyloid-$\beta$ Peptide

Deborah J. Tew,[*‡¶] Stephen P. Bottomley,[§] David P. Smith,[*¶] Giuseppe D. Ciccotosto,[*‡¶] Jeffrey Babon,[‖] Mark G. Hinds,[‖] Colin L. Masters,[†¶] Roberto Cappai,[*†‡¶] and Kevin J. Barnham[*‡¶]

[*]Department of Pathology, [†]Centre for Neuroscience, [‡]Bio21 Molecular Science and Biotechnology Institute, The University of Melbourne, Parkville, Victoria, Australia; [¶]The Mental Health Research Institute of Victoria, Parkville, Victoria, Australia; [§]Department of Biochemistry and Molecular Biology, Monash University, Victoria, Australia; and [‖]Walter and Eliza Hall Institute of Medical Research, Parkville, Victoria, Australia

ABSTRACT An emerging paradigm for degenerative diseases associated with protein misfolding, such as Alzheimer's disease, is the formation of a toxic species due to structural transitions accompanied by oligomerization. Increasingly, the focus in Alzheimer's disease is on soluble oligomeric forms of the amyloid-$\beta$ peptide (A$\beta$) as the potential toxic species. Using a variety of methods, we have analyzed how sodium dodecyl sulphate (SDS) modulates the folding of A$\beta$40 and 42 and found that submicellar concentrations of SDS solubilize A$\beta$ and induce structural transitions. Under these conditions, A$\beta$40 and 42 are interconverting oligomeric ensembles with a predominantly $\beta$-sheet structure. The A$\beta$42 soluble oligomers form $\beta$-sheet structures more readily and have increased stability compared with A$\beta$40 under identical conditions. The presence of added $Cu^{2+}$ significantly promotes and stabilizes the formation of the soluble oligomeric $\beta$-sheet structures but these structures are nonamyloidogenic. In contrast, in the absence of added $Cu^{2+}$, these $\beta$-sheet oligomers possess the hallmarks of amyloidogenic structures. These SDS-induced $\beta$-sheet forms of A$\beta$, both in the presence and absence of $Cu^{2+}$, are toxic to neuronal cells.

## INTRODUCTION

Amyloid-$\beta$ peptide (A$\beta$) is the major component of extracellular neuritic plaques, which are one of the major pathological hallmarks of Alzheimer's disease (1,2). A$\beta$ is produced by the proteolytic cleavage of the transmembrane amyloid precursor protein to form predominantly A$\beta$40 and A$\beta$42 (1). As the progression of AD is marked by neurodegeneration, an early hypothesis was that the accumulating fibrillar A$\beta$ deposits were neurotoxic (3,4). This neurotoxicity was the result of a gain of toxic function as a consequence of A$\beta$ undergoing a conformational transition to a predominantly $\beta$-sheet structure accompanied by peptide aggregation. Further evidence in support of the amyloid hypothesis of AD was the identification of a number of mutations linked to early onset familial AD (5–9). However, there is poor correlation between amyloid plaque burden and disease progression (10–12). More recent evidence has identified smaller soluble $\beta$-sheet-rich oligomers of A$\beta$ as more neurotoxic than amyloid fibrils (13–20) and are more likely to be the toxic agent (16,21–23) responsible for the observed neurodegeneration. There is strong correlation between loss of synaptic terminals and cognitive decline and the presence of such oligomers (24).

Numerous studies have been undertaken to examine the structural transitions of A$\beta$ and the associated gain of toxic function, but interpretation of these studies has been complicated by the tendency of A$\beta$ to form insoluble aggregates which are difficult to study. We have identified solution conditions, using submicellar concentrations of sodium dodecyl sulphate (SDS), that allow the generation of soluble $\beta$-sheet conformers of A$\beta$ (40 and 42) that are more toxic to cultured neuronal cells than freshly prepared solutions of A$\beta$. Similar conditions have recently been reported to generate so-called A$\beta$1-42 globulomers and a 16–20 kDa A$\beta$ oligomer (25).

The aqueous solubility of these $\beta$-sheet rich, soluble oligomers has allowed the use of a number of techniques including circular dichroism (CD) nuclear magnetic resonance (NMR), size-exclusion chromatography, isothermal calorimetry (ITC), and fluorescence spectroscopy to further characterize these species. Data obtained are consistent with the existence of a number of species undergoing conformational or chemical exchange, rather than existing in a single conformational state. The structural transitions observed for A$\beta$40 are reversible, while those for A$\beta$42 (which has a greater tendency to form $\beta$-sheet structures) are not fully reversible. Also, the presence of $Cu^{2+}$ ions, implicated in the pathology of AD (26), is able to significantly stabilize the $\beta$-sheet oligomeric forms and promote a nonamyloidogenic pathway.

## MATERIALS AND METHODS

All chemicals were purchased from Sigma (St. Louis, MO) unless otherwise stated.

### Peptides

Synthetic A$\beta$42 and A$\beta$40 were purchased from W. M. Keck Laboratory (Yale University, New Haven, CT) in lyophilized form.

*Submitted August 15, 2007, and accepted for publication November 1, 2007.*

Address reprint requests to Kevin J. Barnham, E-mail: kbarnham@unimelb.edu.au.

David P. Smith's current address is Institute of Molecular and Cellular Biology, University of Leeds, Leeds, United Kingdom.

Editor: Kathleen B. Hall.



0006-3495/08/04/2752/15 $2.00

doi: 10.1529/biophysj.107.119909

All $Cu^{2+}$ solutions were prepared in solution of one-part $CuCl_2$ to six-parts glycine. The addition of glycine counterions was essential to prevent the formation of insoluble phosphate-metal complexes. The copper concentrations were determined by inductively coupled plasma-mass spectrometry (ICP-MS).

### *Peptide preparation*

Dry peptide was weighed and dissolved in 1,1,1,3,3,3-hexafluoro-2-isopropanol (HFIP) and incubated at 25°C for 1 h to remove any preformed aggregates. It was then aliquoted into small amounts and dried using a speed-vac. The dry peptide was stored at −80°C. Aliquots to be used were dissolved in 1/10 final volume of 20 mM NaOH. This was diluted with phosphate buffer, pH 7.4, followed by sonication with a probe at 0.5 s intervals for 1 min at 30% power, or in a sonicating water bath, chilled with ice, for 15 min. The solution was then centrifuged in a benchtop centrifuge at 13,000 rpm for 20 min. The supernatant was stored on ice until used. Initial peptide concentrations were determined by amino-acid analysis and subsequently the extinction coefficients which were derived for absorbance at 214 nm were 55,771 liters/mol per centimeter for A$\beta$40 and 75,887 liters/mol per centimeter for A$\beta$42.

## CD spectroscopy

CD spectra were obtained using a model No. 810 spectropolarimeter (JASCO, Tokyo, Japan) at 37°C. Far-UV CD spectra were obtained from 190 to 260 nm with a 1-mm pathlength. The baseline acquired in the absence of peptide was subtracted, and the resulting spectra were smoothed using a Fourier transform.

### *SDS titrations*

A$\beta$ was prepared as described and concentration adjusted to 20 $\mu$M. Two-hundred microliters of A$\beta$ was placed in a 0.1-cm cuvette. A stock solution of 35 mM SDS was prepared and was sequentially titrated into the cuvette in aliquots of 1 or 2 $\mu$L. CD spectra were measured as described.

Alpha-cyclodextrin is a cyclohexose able to sequester a wide range of apolar molecules, including SDS, in its hydrophobic interior (27). The complexation reaction is driven by several factors, including desolvation of the guest molecule, van der Waals host-guest interactions, and extensive reorganization of the $\alpha$-cyclodextrins hydrogen-bond network upon complexation (28). Two molecules of $\alpha$-cyclodextrin have been shown to strip one molecule of bound SDS rapidly from proteins. To assess reversibility of the conformational changes induced by SDS, $\alpha$-cyclodextrin was prepared in stock solution at 100 mM and titrated into 20 $\mu$M solutions of A$\beta$40 or A$\beta$42 containing 3 or 8 mM SDS. The data were expressed as effective SDS concentrations, allowing for two molecules of $\alpha$-cyclodextrin to sequester each molecule of SDS. All titrations were carried out at 37°C.

The data obtained from the titrations was analyzed using a three-state model of folding (29), but because the process was not reversible, this fitting procedure was only used to obtain midpoints for each transition.

### *Thermal unfolding*

Thermal unfolding of the peptide (concentration of 0.02 mg/ml) was monitored by the changes in secondary structure as a function of temperature, measured by monitoring the CD signal at 203 nm. A heating rate of 60°C/h was used and the temperature within the cuvette was maintained by a Peltier-driven, computer-controlled water bath connected to a water jacket integral to the cuvette holder and monitored by a sensor directly located in the holder. The second derivative of the resulting data was then used to calculate the inflection point of the transition and hence the midpoint for the thermal transition. Full CD spectra were measured at 5°C intervals to compare the secondary conformations.

## Synchrotron radiation circular-dichroism (SRCD) spectroscopy

Synchrotron radiation circular-dichroism (SRCD) spectra were collected on station 12.1 at the Daresbury Synchrotron Radiation Source. Data were collected at 37°C in a 0.01-cm fused silica cell, with a peptide concentration of 90 $\mu$M and SDS concentrations, as required. Data were collected between 170 and 260 nm, and background readings of buffer in the absence of peptide were subtracted. CD and SRCD spectra were deconvoluted using the DICROWEB website (30,31) using the CONTIN program (32).

## Neurotoxicity

### *Primary neuronal cultures*

Cortical neuronal cultures were prepared as described previously under sterile conditions (33). Briefly, embryonic-day-14 BL6J × 129sv mouse cortices were removed, dissected free of meninges, and dissociated in 0.025% (w/v) trypsin (Sigma) in Krebs buffer. The dissociated cells were triturated using a filter-plugged fine pipette tip, pelleted, resuspended in plating medium (minimum Eagle's medium, 10% fetal calf serum, 5% horse serum), and counted. Cortical neuronal cells were plated into poly(D-lysine)-coated 48-well plates at a density of 150,000 cells/well in plating medium. All cultures were maintained in an incubator set at 37°C with 5% $CO_2$. After 2 h, the plating medium was replaced with fresh neurobasal medium containing B27 supplements, geneticin, and 0.5 mM glutamine (all tissue culture reagents were purchased from Invitrogen, Carlsbad, CA, unless otherwise stated). This method resulted in cultures highly enriched for neurons (>95% purity) with minimal astrocyte and microglial contamination, as determined by immunostaining of culture preparations using specific-marker antibodies (data not shown).

Stuarosporine and copper chloride were purchased from Sigma. $H_2O_2$ and glycine were purchased from BDH (VWR International, BDH Merck, Poole, Dorset, UK). The quantity 10 × PBS refers to Dulbecco's 10× phosphate-buffered saline consisting of 26.67 mM KCl, 14.71 mM $KH_2PO_4$, 1379.3 mM NaCl, and 80.60 mM $Na_2HPO_4$-$7H_2O$.

For use in the neuronal cell viability assays the HFIP-treated dry peptides were dissolved 20 mM NaOH, sonicated for 15 min in an iced waterbath then diluted in 10× PBS and deionized $H_2O$ at v/v/v ratio of 2:7:1. The solution was then centrifuged in a benchtop centrifuge at 13,000 rpm for 20 min. The supernatant was stored on ice until used.

### *Cell viability assays*

The neuronal cells were allowed to mature for six days in culture before commencing treatment using freshly prepared neurobasal medium plus B27 supplements minus antioxidants. For the treatment of neuronal cultures, freshly prepared soluble A$\beta$ stock solutions were diluted to the final concentration in neurobasal medium. The mixtures were then added to neuronal cells for up to four days. Cell survival was monitored by phase contrast microscopy, and cell viability was quantitated using the MTS assay as described previously (33). Briefly, the medium was replaced with fresh neurobasal medium supplemented with B27 lacking antioxidants, and 10% v/v MTS (Promega, Madison, WI) was added to each well and incubated for 3–4 h at 37°C in a 5% $CO_2$ incubator. Plates were gently shaken, and a 100-$\mu$l aliquot from each well was transferred to separate wells of a 96-well plate. The color change of each well was determined by measuring the absorbance at 490 nm using a Wallac Victor Multireader (Wallac, PerkinElmer, Boston, MA), and background readings of MTS incubated in cell-free medium were subtracted from each value before calculations. The data were normalized and calculated as a percentage of untreated vehicle control values. Data are shown as mean ± SE. Statistical comparisons between groups were done using Student's *t*-test.

## Analysis of aggregate size

The product of the overnight incubations in 1 mM SDS was centrifuged to pellet any insoluble aggregates and the supernatant was applied to a Superose

75 column (Amersham Pharmacia Biotech, Uppsala, Sweden) for separation by size exclusion. Commercial standards, prepared in identical solutions of 1 mM SDS, were used to calibrate the column.

## SDS-PAGE

After overnight incubation at 37°C, with shaking, the samples were resolved by SDS-PAGE. The resolving matrix was a 16% Tris-Glycine SDS gel and the membrane probed with the monoclonal antibody WO2 (34).

## Isothermal calorimetry

Isothermal calorimetric titrations were performed using an Omega VP isothermal titration calorimeter (MicroCal, Northampton, MA). All experiments were performed at 37°C. The data were analyzed using the evaluation software, MicroCal Origin, Ver. 5.0, provided by the manufacturer. The binding curve fitted a single-site binding model in all cases and $K_d$ values were determined from experiments repeated at least twice. This method measures the amount of energy absorbed or released as a result of changes that occur within the calorimeter bulb. For SDS critical micelle concentration (CMC) determination, the calorimeter cell, which has an internal volume of 1.425 ml, contained phosphate buffer plus 2 mM NaOH at pH 7.4. It was titrated with 29 injections of 10 $\mu$l of 56 mM SDS, to determine the CMC under experimental conditions. For determination of the heat of binding of copper, solutions of 20 $\mu$M A$\beta$ in 1 mM SDS in the cell were titrated by injections of a total of 290 $\mu$L 160 $\mu$M $Cu^{2+}$ . The heat of dilution of the $Cu^{2+}$ was subtracted from the raw data of the binding experiment. For determination of the heat of folding of A$\beta$ in SDS, the cell contained phosphate buffer, SDS, and NaOH, as used for the peptide preparation with or without copper ions. This was titrated with five injections of 50 $\mu$L of peptide at 70 $\mu$M. The value of $\Delta H$ for each addition of peptide was plotted against the final peptide concentration and the values were fitted to a linear regression. To ascertain the $\Delta H$ of folding alone without any components of intermolecular interaction, the linear regression was extrapolated to zero to give the true $\Delta H$ of folding and the values shown later in Table 4 (a similar methodology is used to find the $\Delta G$ of unfolding in denaturant, where the unfolded baseline is back-extrapolated to zero denaturant (35)).

## NMR spectroscopy

NMR spectra were recorded at 37°C on a model No. DRX-600 spectrometer (Bruker Optics, Billerica, MA) equipped with triple resonance probes and pulsed field gradients operating at 600 MHz. The A$\beta$40 or A$\beta$42 sample was prepared by dissolving 0.5 mg A$\beta$40 in 55 $\mu$L $^2H_2O$ made up to 630 $\mu$L with 10 mM phosphate buffer pH 6.4. $^{15}$N-labeled A$\beta$40 was purchased from rPeptide (Athens, GA) and made to the same concentration in 10% $^2H_2O$/10 mM phosphate buffer pH 6.4. Spectra were processed and analyzed using XWINNMR (Bruker) or analyzed using XEASY (36).

## Aggregation studies using Thioflavin T (ThT) fluorescence

Thioflavin T (ThT) is routinely used to indicate the presence of $\beta$-sheet amyloidogenic structures. For detection of fibril formation, 10 $\mu$M A$\beta$40 or A$\beta$42 solutions were prepared as above either alone or in the presence of SDS, with and without equimolar $Cu^{2+}$ or $Zn^{2+}$ with 20 $\mu$M ThT. Six-hundred microliters of each sample was incubated at 37°C in a stirred cuvette. The ThT signal was excited at 444 nm and emission was measured at 480 nm. Fluorescence was measured using a Varian Cary Eclipse fluorescence spectrophotometer (Palo Alto, CA) fitted with a Peltier-driven temperature controller and a multicell holder. Readings were taken every 60 s for the first 15 min then every 15 min for the next 885 min. Slit widths were 5 nm for both excitation and emission. In preliminary experiments, we showed that ThT fluorescence is not affected by the presence of SDS.

# RESULTS

## Critical micellar concentration (CMC) determination of SDS

The CMC of SDS can vary depending on solution conditions such as the concentration of counterions in the solution and the temperature (37,38). SDS was titrated into the isothermal calorimeter cell containing 10 mM phosphate buffer at pH 7.4 and 37°C; these buffer and conditions were used for all other experiments. Under these conditions, the CMC of SDS was found to be 3.1 mM, and in the presence of 20 $\mu$M $Cu^{2+}$, the CMC was 3.4 mM (Supplementary Material, Fig. S1).

## Far-UV CD

### *Submicellar SDS induces $\beta$-sheet conformation in A$\beta$40 and A$\beta$42*

Far-UV CD spectra were recorded as SDS was titrated into a buffered aqueous solution of A$\beta$ peptides 1-16 (A$\beta$16), 1-28 (A$\beta$28), 1-40 (A$\beta$40) or 1-42 (A$\beta$42) (Fig. 1). All CD spectra were analyzed using the CONTIN algorithm via the DICHROWEB website (30,32); the results are summarized in Table 1. Spectra obtained in the absence of SDS indicated that all A$\beta$ peptides contained a high percentage of random coil (i.e., conformationally averaged). Titration of SDS into the peptide solutions revealed that although no conformational change was observed in the shortest peptide (A$\beta$16) (Fig. 1 *a*) there was a transition to an $\alpha$-helical structure by A$\beta$28 (Fig. 1 *b*) as the SDS concentration reached the CMC. The helical structure content is consistent with previously reported structural studies using the A$\beta$ peptides in aqueous solutions with high concentrations of SDS (39,40). However, there was no isodichroic point observed for this transition to indicate that the conversion from random coil to $\alpha$-helical structure did not proceed via a simple two-state mechanism.

When SDS was titrated into aqueous solutions containing A$\beta$40, a three-state transition from random coil through a $\beta$-sheet-rich intermediate to an $\alpha$-helical endpoint was observed (Fig. 1 *c*). Under the conditions of this experiment, the folding pathways of A$\beta$40 involved the population of an intermediate $\beta$-sheet-rich conformation at submicellar levels of SDS, while the fully folded product was predominantly $\alpha$-helical in SDS concentrations above the CMC.

To examine the folding of A$\beta$40 as a function of SDS concentration the relative far-UV CD signal measured at 203 nm was plotted against SDS concentration (Fig. 2 *a*). 203 nm was selected because the magnitude of the CD signal is most sensitive to changes in composition of secondary structure. These data indicate that for A$\beta$40 the midpoint of the transition from the random coil-rich conformation to the $\beta$-sheet-rich conformation occurred at ~0.6 mM SDS. Further addition of SDS

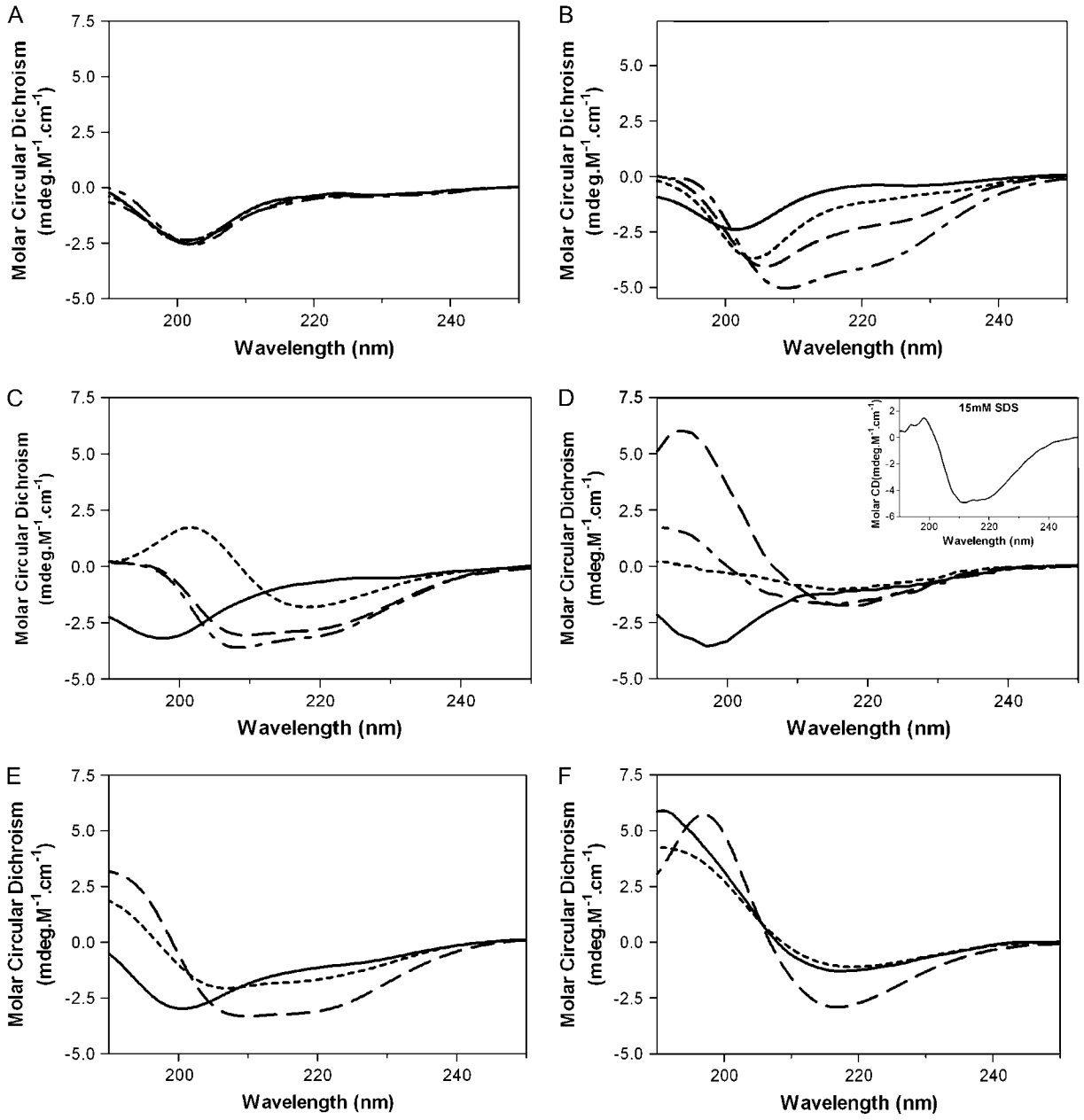


FIGURE 1 CD spectra of Aβ peptides in increasing concentrations of SDS. (*A*) Aβ (1-16), (*B*) Aβ (1-28), (*C*) Aβ40, and (*D*) Aβ42 in phosphate buffer (*solid line*); in 1.5 mM SDS (*line with short dashes*); 3 mM SDS (*line with long dashes*); and 8 mM SDS (*line with alternating short and long dashes*). (*Inset*) CD spectrum of Aβ42 in 15 mM SDS. Units shown are the per-residue molar absorption units of circular dichroism, measured in mdeg $M^{-1}$ $cm^{-1}$ plotted against wavelength in nm. CD spectra in (*E*) Aβ40 and (*F*) Aβ42 showing the effects of decreasing concentrations of SDS when the α-cyclodextrin is titrated into the solution to remove SDS. The effective SDS concentrations shown are: 0 mM (*solid line*); 1.5 mM SDS (*line with short dashes*); and 3 mM SDS (*line with long dashes*).

led to a second conformational change resulting in the fully folded conformation in micellar SDS; the midpoint of the second transition was centered at ~2.3 mM SDS.

### *$Cu^{2+}$ stabilizes β-sheet conformation*

A similar SDS titration was performed in an aqueous solution of Aβ42. Increasing SDS concentration lead to an increase in the β-sheet content of the peptide (Fig. 1 *d*). However, a predominantly α-helical conformation could only be observed at SDS concentrations in excess of 8 mM SDS (see Fig. 1 *d*, *inset*; Aβ42 in 15 mM SDS). The SDS-induced folding of Aβ1-42 also displayed two transitions centered at ~0.4 and 3.1 mM SDS (Fig. 2 *b*). $Cu^{2+}$ ions have been implicated in the pathology of AD and reported to have extensive effects on Aβ structure, chemistry, and biology (26).

**TABLE 1 Deconvolution of CD spectra in varying SDS concentrations**

| A$\beta$ peptide | SDS concentration | $\alpha$-helical content (+Cu) | $\beta$-sheet content (+Cu) | $\beta$-turns (+Cu) | Random coil (+Cu) |
|---|---|---|---|---|---|
| A$\beta$(1-16) | 0 | 10 | 33 | 25 | 32 |
| A$\beta$(1-16) | 1 | 13 | 28 | 26 | 33 |
| A$\beta$(1-16) | 3 | 14 | 27 | 25 | 34 |
| A$\beta$(1-16) | 8 | 12 | 37 | 21 | 30 |
| A$\beta$(1-28) | 0 | 14 | 28 | 24 | 34 |
| A$\beta$(1-28) | 1 | 21 | 23 | 26 | 30 |
| A$\beta$(1-28) | 3 | 28 | 18 | 23 | 31 |
| A$\beta$(1-28) | 8 | 34 | 7 | 26 | 33 |
| A$\beta$(1-40) | 0 | 16 (9) | 25 (34) | 24 (23) | 35 (33) |
| A$\beta$(1-40) | 1 | 1 (3) | 42 (41) | 21 (21) | 36 (34) |
| A$\beta$(1-40) | 3 | 31 (24) | 15 (21) | 22 (23) | 32 (32) |
| A$\beta$(1-40) | 8 | 35 (28) | 11 (19) | 23 (21) | 31 (32) |
| A$\beta$(1-42) | 0 | 15 (8) | 25 (32) | 22 (24) | 38 (36) |
| A$\beta$(1-42) | 1 | 8 (8) | 37 (39) | 22 (21) | 33 (32) |
| A$\beta$(1-42) | 3 | 14 (9) | 39 (39) | 16 (26) | 32 (31) |
| A$\beta$(1-42) | 8 | 16 (7) | 29 (39) | 21 (22) | 34 (33) |
| A$\beta$(1-42) | 15 | 28 | 18 | 21 | 33 |
| $\alpha$-cyclodextrin titration | | | | | |
| A$\beta$(1-40) | 0 | 9 | 32 | 24 | 34 |
| A$\beta$(1-40) | 1 | 14 | 29 | 24 | 32 |
| A$\beta$(1-40) | 3 | 18 | 25 | 25 | 32 |

CD and SRCD spectra were deconvoluted using the DICROWEB website (30,31) using the CONTIN program (32) Values in parentheses are for spectra obtained in the presence of $Cu^{2+}$.

To examine the effect that $Cu^{2+}$ ions had on the folding pathway of A$\beta$, the titrations of SDS into A$\beta$40 and A$\beta$42 were repeated in the presence of one molar equivalent of $Cu^{2+}$ (Fig. 2, *a* and *b*).

Titration of increasing amounts of SDS into a solution of A$\beta$40 containing equimolar concentrations of $Cu^{2+}$ resulted in two structural transitions.

The first transition was to a $\beta$-sheet-rich conformation followed by a transition to increased $\alpha$-helical conformation. While the structural changes observed were unchanged by the presence of $Cu^{2+}$, the concentration of SDS required to induce these structural changes was significantly decreased, indicating that the pathway has been altered. The first transition to a $\beta$-sheet-rich structure is centered at ~0.4 mM SDS while the second transition to an $\alpha$-helical structure occurred at 2.3 mM SDS. The difference in midpoints observed in the presence (0.4 mM) and absence (0.6 mM) of $Cu^{2+}$ indicates the transition from native random coil to the $\beta$-sheet-rich intermediate state occurred at lower SDS concentration in the presence of $Cu^{2+}$, with a qualitative estimated $\Delta\Delta G$ of ~−4.0 kcal/mol. The SDS-induced folding curves were fitted to a three-state model, using a nonlinear, least-squares fitting algorithm (29), the analysis of which suggests that the energy required for the transition from unfolded structure to a $\beta$-sheet conformation is significantly lower in the presence of $Cu^{2+}$. CD spectra (see Supplementary Material, Fig. S2) also showed that the presence of $Cu^{2+}$ induced an increase in local structure in the peptide consistent with the concept that $Cu^{2+}$ stabilized the $\beta$-structure. When SDS was titrated into a solution of A$\beta$42 containing equimolar $Cu^{2+}$ there was a shift in the amount of SDS required to induce the structural transitions. Once again, less SDS was required to initiate the first transition while more SDS was required for the second transition. The $\Delta\Delta G$ induced by the presence of $Cu^{2+}$ was ~1.4 kcal/mol, which is lower than that observed for A$\beta$40, which reflects the increased $\beta$-sheet content in the presence

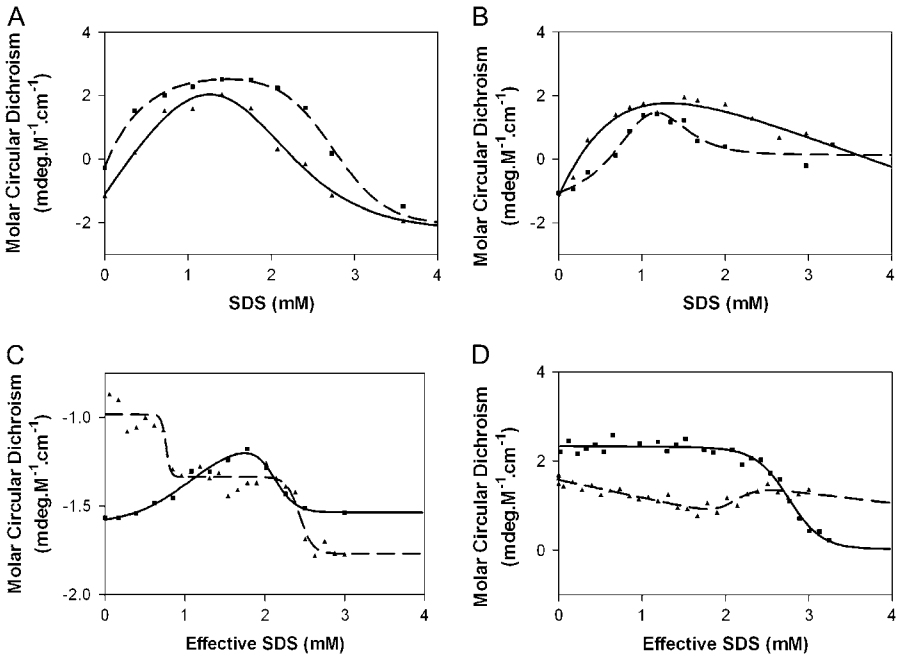


FIGURE 2 Folding and unfolding curves. (*A*) A$\beta$40 and (*B*) A$\beta$42 folding when SDS was titrated into solution in the absence (*squares*) or presence (*triangles*) of equimolar $Cu^{2+}$. The molar circular dichroism measured at 203 nm was plotted against the SDS concentration. (*C*) A$\beta$40 and (*D*) A$\beta$42 unfolding as $\alpha$-cyclodextrin was titrated into the solution containing SDS in the absence (*squares*) or presence (*triangles*) of equimolar $Cu^{2+}$. The molar circular dichroism measured at 203 nm was plotted against the effective SDS concentration. The data in *A*, *B*, and *C* were fitted to a three-state model of folding (29); the data in *D* was fitted to a two-state model of folding (35). On each graph these are represented by a solid line in the absence of $Cu^{2+}$ and a dashed line in the presence of $Cu^{2+}$.

of $Cu^{2+}$ by Aβ42 in buffer. The addition of submicellar concentrations of SDS did not induce any additional increase the overall β-sheet content (Table 1).

A second transition was observed at higher SDS concentrations, but in the SDS concentration range used for the titrations, a fully α-helical conformation was not observed. In fact, in the presence of $Cu^{2+}$ this second transition resulted in a significant increase in the β-sheet content of Aβ42. Therefore, the presence of $Cu^{2+}$ had rendered the β-sheet conformation extremely stable.

### *Alpha-cyclodextrin reverses SDS-induced conformational changes*

Two molecules of α-cyclodextrin have been shown to strip one molecule of bound SDS rapidly from proteins (27). Therefore, to assess reversibility of the conformational changes induced by SDS, α-cyclodextrin was titrated into aqueous SDS solutions of Aβ40 and Aβ42. When α-cyclodextrin was titrated into the peptide solution in the absence of SDS, no conformational changes to either peptide was observed—indicating that there is no direct interaction between α-cyclodextrin and Aβ. Both Aβ40 and Aβ42 were prepared in micellar SDS, and α-cyclodextrin was titrated into the solutions. The Aβ40 was in an α-helical conformation in micellar SDS, and returned to a β-sheet-rich state in submicellar SDS as the α-cyclodextrin was titrated into the solution. The midpoint of this transition was 2.0 mM SDS concentration (corresponding well with the midpoint of the β-sheet to α-helix transition), demonstrating that this transition was fully reversible. Further addition of α-cyclodextrin also showed that the transition from β-sheet-rich conformation to random coil was clearly evident for the Aβ40 peptide, with the transition centered at ~1.2 mM SDS. This is higher than the midpoint of the folding from random coil to β-sheet-rich intermediate, which had a midpoint of 0.3 mM—indicating that this change is not fully reversible, and may proceed via a different unfolding pathway.

These titrations were repeated for Aβ42 and there was a structural transition to a more β-sheet-rich structure as the apparent concentration of SDS decreased to below the CMC. The midpoint of this transition was 2.8 mM SDS. Further addition of α-cyclodextrin did not induce a transition to a predominately random coil conformation, which is an indication of the inherent stability of the β-sheet conformation for Aβ42. The starting Aβ42 solution was in 4 mM SDS for these experiments, but it was prepared from peptide dissolved in higher concentrations of SDS. It differed in conformation from the endpoint peptide in the corresponding titration, which increased the SDS concentration and showed a large proportion of persistent β-sheet. The hysteresis in folding of Aβ42 in SDS occurred because the β-rich conformation is a kinetic trap for the folding of Aβ42. Representative CD spectra from the α-cyclodextrin titration are shown in Fig. 1, *e* and *f*.

The α-cyclodextrin titrations were repeated in the presence of $Cu^{2+}$. The CD changes at 203 nm were plotted as a function of SDS concentration (Fig. 2, *c* and *d*). These data show that there are clearly different pathways for folding and unfolding in the presence of $Cu^{2+}$. The midpoints of the folding and unfolding transitions are shown in Table 2. These results show that, in the presence of $Cu^{2+}$, there were significant differences in the midpoints of unfolding transitions compared to the folding transitions (i.e., they are not reversible). This indicates that the structural differences induced by the presence of $Cu^{2+}$ alter the folding and unfolding pathways. With respect to Aβ42; $Cu^{2+}$ stabilized the intermediate β-sheet conformation to such an extent that the peptide did not unfold completely, and a significant proportion of β-sheet persisted in the final conformation free of SDS.

### *Thermal denaturation from β-sheet or α-helical conformations*

The relative stabilities of the β-sheet-rich intermediates and α-helical conformations were tested by performing thermal denaturation experiments. When Aβ40 in 1 mM SDS was heated at 1°C per min, the β-sheet conformation was lost and the CD spectrum at 90°C had a minimum at 200 nm, which is diagnostic of being structurally undefined. The midpoint of transition ($T_m$) was 41°C. The solution was then slowly cooled and the β-sheet conformation was restored with a similar $T_m$, showing that the conformational change from β-sheet to a structurally undefined form was reversible. When the Aβ40 was dissolved in micellar 3 mM SDS, the CD spectra had double minima at 208 and 222 nm, indicating an α-helical conformation. Thermal denaturation of the α-helical structure to a random coil conformation occurred with a single transition, with a $T_m$ of 51.5°C (Fig. 3 *a*), and when the sequential CD spectra were overlaid, they revealed an isodichroic point. The presence of an isodichroic point is indicative of the presence of only two conformational states populating the thermally induced unfolding pathway. When cooled, the α-helical conformation was restored with a similar $T_m$, indicating the reversibility of the conformational change.

**TABLE 2 Midpoints of conformational transitions**

| | Midpoints of conformational transitions (mM SDS) | | | |
|---|---|---|---|---|
| | SDS titration | | α-CD titration | |
| Peptide | Buffer → submicellar SDS | Submicellar → micellar SDS | Micellar → submicellar SDS | Submicellar SDS → buffer |
| 1-40 | 0.6 | 2.29 | 2.1 | 1.1 |
| 1-40 + Cu | 0.4 | 2.75 | 2.4 | 0.9 |
| 1-42 | 0.4 | 3.11 | 2.8 | |
| 1-42 + Cu | 1 | 1.47 | 2.1 | |

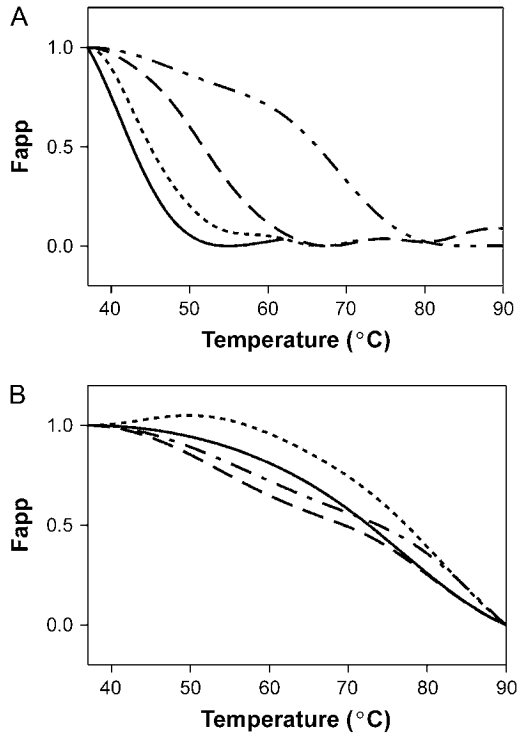


FIGURE 3 Thermal denaturation of A$\beta$ peptides in SDS; The thermal denaturation was followed using circular dichroism in the far-UV region at 195 nm, which was plotted as ''Fapp'' (the apparent fraction folded) against temperature. The curves were smoothed using a Fourier transform. (*A*) A$\beta$40 and (*B*) A$\beta$42, peptides in 1 mM SDS (*solid line*); 1 mM SDS + $Cu^{2+}$ (*line with short dashes*); 3 mM SDS (*line with long dashes*); and 3 mM SDS + $Cu^{2+}$ (*line with alternating short and long dashes*).

### *$\beta$-sheet conformation in 1 mM SDS is resistant to thermal denaturation*

In 1 mM SDS, A$\beta$42 displayed a $\beta$-sheet structure, but upon heating to 90°C, it lost some of its structure; however, the conformation was still predominantly $\beta$-sheet at 90°C. The $T_m$ for this transition was 82°C. When cooled, the $\beta$-sheet conformation was restored, but the $T_m$ was 65°C. Interestingly, the CD spectrum of the refolded peptide in 1 mM SDS after heating showed a higher CD signal maximum at 198 nm. It is possible that the loss of structure at 90°C represented a loss of the residual aggregation present in the starting solution, and that the final solution is a more homogeneous solution of small $\beta$-rich oligomers. When A$\beta$42 was dissolved in 3 mM SDS, it retained some $\beta$-sheet conformation (Figs. 1 and 2). When this mixture was heated to 90°C, there was a sloping baseline which was probably due to disruption of the SDS micelles, or small oligomers. There was also a transition with a $T_m$ of 80°C. When this mixture was cooled to 37°C, there was a single transition with $T_m$ of 63°C. The CD spectra measured before and after these melts overlaid completely, indicating that the secondary conformation before and after melting was unchanged. The hysteresis observed suggests that the unfolding involved overcoming a kinetic barrier, such as dissociating oligomeric species, whereas the folding was a cooperative event. By contrast, when the A$\beta$42 was dissolved in 15 mM SDS, the conformation was a mixture of $\alpha$-helix and $\beta$-sheet. Upon heating to 90°C, the conformation had an increased amount of random coil. The midpoint of this transition was 67.7°C (Fig. 3 *b*). When this was cooled, the CD spectrum indicated that the peptide returned to its original conformation with a similar $T_m$ (Table 3).

### *Thermal stability is further increased by $Cu^{2+}$*

The thermal melts for both peptides in 1 mM and 3 mM SDS were repeated in the presence of $Cu^{2+}$, and an increase in the $T_m$, consistent with the $Cu^{2+}$ ions stabilizing the secondary structure was observed. The CD signal measured at 195 nm was plotted against temperature for A$\beta$40 and A$\beta$42 in the absence and presence of $Cu^{2+}$, and the results are shown in Fig. 3. The midpoints of the various transitions are shown in Table 3.

## Isothermal calorimetry

### *Small heat of conformational change ($\Delta$H) when $\beta$-sheet-rich intermediate is formed*

ITC measures the energy change as a result of conformational change or the binding of a ligand. When A$\beta$40 was titrated into 1 mM SDS at 37°C, there was very little heat change observed ($\Delta H \sim -0.3$ kcal/mol), which is in agreement with the thermal denaturation studies showing a $T_m$ of 41°C (i.e., only a small amount of heat was needed to cause the conformational change from random coil to $\beta$-sheet). The A$\beta$42 peptide had a $T_m$ of 45°C, and it also displayed little heat change with $\Delta H \sim -0.8$ kcal/mol.

### *Submicellar SDS conformation significantly stabilized in the presence of $Cu^{2+}$*

The titrations were repeated in the presence of $Cu^{2+}$ (Fig. 4 *b*). The value of $\Delta H$ for each addition of peptide was plotted

**TABLE 3 Midpoints of thermal denaturations**

| Peptide | SDS concentration (mM) | Midpoints of transition 37–90°C ($T_m$ 37–90) | Midpoints of transition 90–37°C ($T_m$ 90–37) |
|---|---|---|---|
| A$\beta$(1-40) | 1 | 41 | 41 |
| A$\beta$(1-40) + $Cu^{2+}$ | 1 | 42.8 | 40 |
| A$\beta$(1-40) | 3 | 51.5 | 51.5 |
| A$\beta$(1-40) + $Cu^{2+}$ | 3 | 48 and 69 | 50 and 69.9 |
| A$\beta$(1-42) | 1 | 77 | 45.8 |
| A$\beta$(1-42) + $Cu^{2+}$ | 1 | 81.9 | 65.5 |
| A$\beta$(1-42) | 3 | 53.8 and 80.2 | 62.9 |
| A$\beta$(1-42) + $Cu^{2+}$ | 3 | 58.1 and 86.3 | 69.2 |
| A$\beta$(1-42) | 15 | 67.7 | |

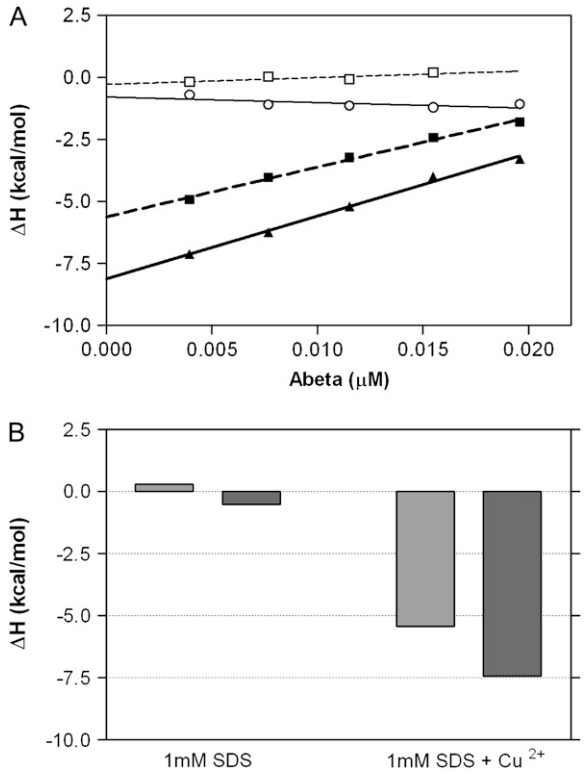


FIGURE 4 ITC titrations. (*A*) Aβ40 (*dash-square-dash line*) or Aβ42 (*dash-circle-dash line*) were titrated into the calorimeter bulb (MicroCal) at 37°C containing 1 mM SDS; or Aβ40 (*dash-square-dash line*) or Aβ42 (*dash-circle-dash line*) were titrated into the calorimeter bulb at 37°C containing 1 mM SDS and $Cu^{2+}$. The resulting $\Delta H$ values were plotted as a function of the final concentration of peptide. This was fitted to a linear regression and extrapolated to zero to determine the $\Delta H$ for peptide titrated into 1 mM SDS alone or in the presence of an excess of $Cu^{2+}$. (*B*) Titration of Aβ40 (*shaded representation*) and Aβ42 (*solid representation*) into 1 mM SDS, 1 mM SDS plus excess $Cu^{2+}$. SDS was titrated into 10 mM phosphate buffer with 2 mM NaOH at pH 7.4 at 37°C. Midpoint of transition is at 3.0 mM SDS.

against the final peptide concentration and the values were fitted to a linear regression. The linear regression was extrapolated to zero to give the true $\Delta H$ of folding and the values shown in Table 4. (A similar methodology is used to find the $\Delta G$ of unfolding in denaturant, where the unfolded baseline is back-extrapolated to zero denaturant (35).) When the effects of SDS alone were subtracted, the heat of binding to copper resulted in a difference in $\Delta H$ of $-5.3 \pm 0.1$ kcal/mol for Aβ40 and $-7.3 \pm 0.2$ kcal/mol for Aβ42. The ITC results are in agreement with the CD data, demonstrating that the presence of $Cu^{2+}$ ions significantly stabilized the intermediate, β-sheet- rich conformation populated in submicellar concentrations of SDS. The $\Delta H$ values calculated from titration of the peptides into submicellar SDS in the presence or absence of copper ions differed, and it follows that this difference arises from differences in the conformational changes in the peptides. This supports the notion that the folding pathways for the peptides in the presence and absence of copper are dissimilar.

**TABLE 4 $\Delta H$ kcal/mol of structural changes in Aβ peptides in 1 mM SDS and for binding of Aβ peptides to $Cu^{2+}$ in 1 mM SDS**

| | 1 mM SDS | 1 mM SDS + Cu |
|---|---|---|
| Aβ(1-40) | $-0.3 \pm 0.1$ | $-5.6 \pm 0.1$ |
| Aβ(1-42) | $-0.8 \pm 0.2$ | $-8.1 \pm 0.1$ |

### *Thermal parameters associated with binding $Cu^{2+}$ to the β-sheet-rich conformation*

Another set of titrations was carried out in which the Aβ40 or Aβ42 in 1 mM SDS solution were present in the bulb of the ITC calorimeter and $Cu^{2+}$ was titrated in small increments, to determine the thermal parameters associated with the binding of $Cu^{2+}$ . The thermal parameters provided $\Delta H$ and $\Delta S$, from which $\Delta G$ and $K$ could be calculated using Origin software. The data, shown in Table 5, are global figures reflecting the combined effects of a number of different processes including the coordination of $Cu^{2+}$ and the subsequent structural transitions induced by the copper. As can be seen, the $\Delta H$ and $\Delta G$ for binding of copper to both peptides were similar when the peptides were already in the presence of submicellar SDS, reflecting that the metal-binding event was similar in each case.

## NMR spectroscopy

### *Submicellar SDS induces a dynamic equilibrium of interchanging species*

Nuclear magnetic resonance (NMR) spectra were recorded for Aβ40 and 42 in an aqueous environment, at submicellar SDS (1 mM) and above the SDS CMC (Fig. 5). The $^1$H NMR spectrum of Aβ40 in aqueous solution was indicative of a peptide of 4.3 kDa molecular mass (Fig. 5 *a*). The titration of SDS to a final concentration of 1 mM induced line-broadening of the spectrum of Aβ40, indicating either the presence of a dynamic equilibrium of interchanging species broadening the resonances and/or an aggregation process (Fig. 5 *b*). Resonances due to the SDS were also significantly broadened at the submicellar concentration, indicating that the SDS was interacting with the Aβ assembly. The addition of metal ions had no effect on the broadened resonances observed at submicellar SDS (data not shown). The addition of further SDS beyond the CMC caused a further structural transition and of the $^1$H NMR spectrum, reflecting the formation of the expected α-helical Aβ40 as previously described (40,41). This is further demonstrated by the $^1$H-$^{15}$N HSQC spectra of Aβ40. Before addition of SDS, there is a relatively small dispersion of amide resonances, and after addition of SDS to a final concentration of 8 mM, there is increased spectral dispersion (see Supplementary Material, Fig. S3). At the intermediate concentration of SDS, the broadening of the HSQC peaks was so severe that no peaks were observed.

**TABLE 5 Thermal parameters derived by titrating $Cu^{2+}$ into solutions of A$\beta$ in 1 mM SDS**

| Peptide | $\Delta H$ in A$\beta$ titration into 1 mM SDS (kcal/mol) | $\Delta H$ in A$\beta$ titration into 1 mM SDS and Cu (kcal/mol) | Peptide | $\Delta\Delta H$ (kcal/mol) | $\Delta S$ (kcal/mol/°C) | $\Delta G$ (kcal/mol) | $K$ |
|---|---|---|---|---|---|---|---|
| A$\beta$ (40) | 0.1 | −5.6 ± 0.1 | A$\beta$(1-40) | −6.9 ± 0.1 | 2.73 | −8.8 | 486,000 ± 3220 |
| A$\beta$ (42) | −0.5 | −8.1 ± 0.1 | A$\beta$(1-42) | −7.4 ± 0.2 | 6.07 | −8.2 | 638,000 ± 54,400 |

These figures were obtained using the software ORIGIN (MicroCal) to analyze the isothermal titration calorimetry (ITC) data obtained using a Microcal VP-ITC instrument, and reflect the combined effects of a number of different processes including the coordination of $Cu^{2+}$ and the subsequent structural transitions induced by the copper.

A$\beta$40 in the absence and presence of SDS is structured as shown by the $^{1}H,^{15}N$ HSQC (see Supplementary Material, Fig. S3). Similar results were achieved with A$\beta$42 (data not shown).

## Fluorescence studies

### *ThT-active structures induced in submicellar SDS environment*

Thioflavin-T (ThT) fluorescence was used to monitor the presence of amyloidogenic material in solutions of A$\beta$40 and A$\beta$42 in the presence and absence of SDS and $Cu^{2+}$ ions (Fig. 6, *a* and *b*). A$\beta$40 did not form ThT-positive species in the absence of SDS during an overnight incubation, with or without the addition of $Cu^{2+}$. Similarly, in the presence of 3 mM SDS, A$\beta$40 did not form ThT-active species. In 1 mM (submicellar) SDS, ThT-active species were formed, indicating the presence of amyloidogenic-like material; however, in the presence of $Cu^{2+}$ ions, the formation of ThT-active species was inhibited (Fig. 6 *a*). After overnight incubation in the presence of $Cu^{2+}$, EDTA was added to sequester the $Cu^{2+}$ ions, to determine whether the lack of ThT fluorescence was due to quenching of the ThT signal. There was only a small increase in signal in the presence of EDTA, indicating that, while there was some quenching of the fluorescence by $Cu^{2+}$, the level of fluorescence was low, because the stable $\beta$-sheet-rich structures formed in the presence of $Cu^{2+}$ were not ThT-active.

A$\beta$42 in aqueous buffer rapidly formed a small amount of ThT-active species, possibly seeded by preexisting oligomers, but in 8 mM SDS it was unable to form a ThT-active species. In 1 mM SDS, A$\beta$42 rapidly formed a large amount of ThT-active species. To find the solubility of the ThT-positive species, the mixtures were centrifuged at 13,000 *g* for 20 min after the aggregation assay to pellet any insoluble (fibrillar) material, and the fluorescence emission spectra of the supernatant fractions were determined. As shown in Fig. 6 *d*, 90% of the ThT fluorescence of the peptide in 1 mM SDS was present in the soluble fraction, while only 50% of the

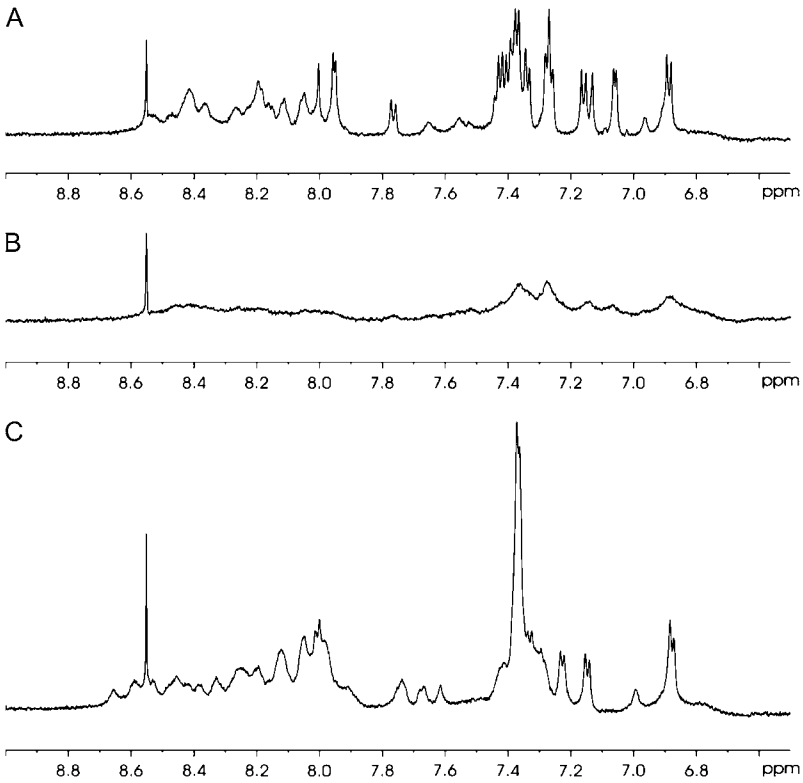


FIGURE 5 $^{1}H$ NMR spectra of A$\beta$40. (*A*) In aqueous solution, (*B*) in the presence of 1 mM SDS, and (*C*) micellar SDS.

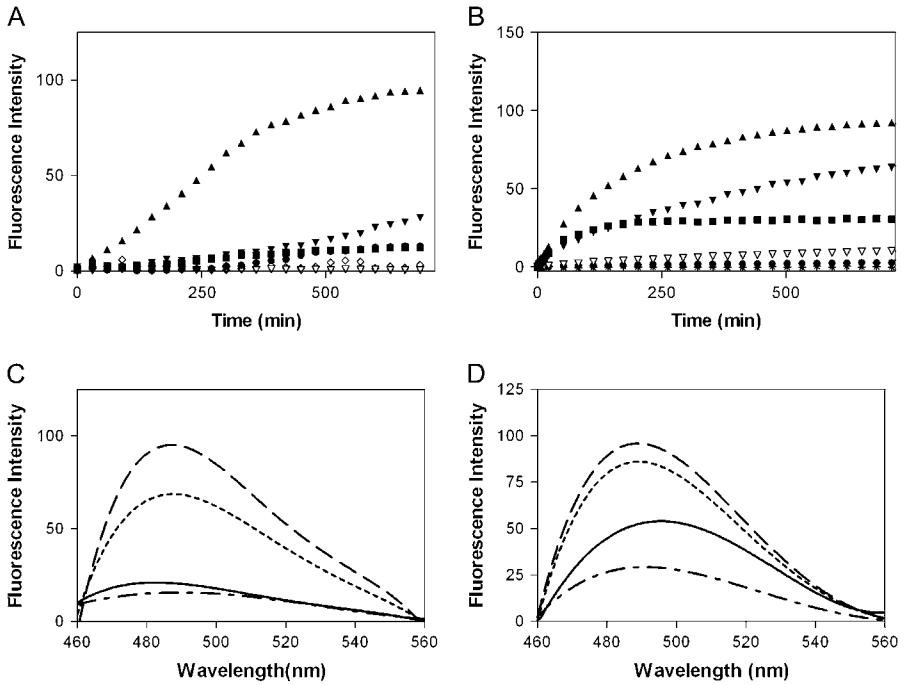


FIGURE 6 Thioflavin-T (ThT) fluorescence in the presence or absence of Aβ peptides and metal ions; growth of ThT-active oligomers was monitored using ThT fluorescence. The fluorescence was plotted against time. (*A*) Aβ40 and (*B*) Aβ42 in phosphate buffer (■); in 1 mM SDS (▲); 1 mM SDS + $Cu^{2+}$ (∇); PB + $Cu^{2+}$ (●); 3 mM SDS (▼); and 8 mM SDS (*). Spectra of ThT fluorescence in (*C*) Aβ40 and (*D*) Aβ42 measured after overnight incubations at 37°C, total sample in buffer (*solid line*); supernatant of sample in buffer after centrifugation (*line with alternating short and long dashes*); total sample in 1 mM SDS (*line with long dashes*); and supernatant of sample in 1 mM SDS after centrifugation (*line with short dashes*).

ThT fluorescence of peptide in buffer resided in the soluble fraction. As observed with Aβ40, the presence of $Cu^{2+}$ ions inhibited the formation of ThT-active species. Analysis of the SDS titrations by far-UV CD showed that the maximum β-sheet content occurred at ~1 mM SDS. These data indicate that this species corresponds to a ThT-positive, soluble β-sheet-rich species, which is stable even after overnight incubation at 37°C in 1 mM SDS.

## Size-exclusion chromatography

### *Analysis of aggregate size indicates presence of oligomers*

The products of the overnight incubations in 1 mM SDS were centrifuged to pellet any insoluble aggregates and the supernatant were applied to a Superose 75 column (Amersham Pharmacia Biotech) for separation by size exclusion. Commercial standards, prepared in identical solutions of 1 mM SDS, were used to calibrate the column.

The Aβ40 samples (Fig. 7 *a*) had a small peak corresponding to an apparent weight of ~4 kDa (monomer); however, the majority of the protein was present as a mixture of small oligomeric species with apparent weights between 9 and 15 kDa and a small peak with a higher weight of ~70 kDa. In the presence of $Cu^{2+}$, there were peaks with apparent weights between 9 and 15 kDa; however, the elution profile is different from that produced in the absence of $Cu^{2+}$, consistent with the oligomers having different conformations, as indicated by the ThT fluorescence studies (see above).

Aβ42 in 1 mM SDS (Fig. 7 *c*) showed a very large percentage of the product at a much higher molecular-weight range, predominantly in the region of 60–70 kDa, with smaller peaks in the 12 and 4 kDa regions. Interestingly, the 38–48 KDa ''globulomers'' produced by Baghorn et al. (25) also eluted from size-exclusion chromatography in the same molecular-weight range. The elution profile upon addition of $Cu^{2+}$ showed a decrease in the peak at 70 kDa.

After overnight incubation at 37°C, with shaking, the samples were resolved by SDS-PAGE, transferred to nitrocellulose membranes, and analyzed by Western blotting with the WO2 antibody (Fig. 8). The Aβ40-alone sample (Fig. 8, lane 1) migrated as a smear, with distinct bands corresponding in molecular mass to monomer, dimer, and trimer species, plus higher-weight oligomers at 50 kDa and greater. The Aβ42-alone reaction displayed a different pattern than Aβ40, with distinct monomer, trimer, and tetramer bands, plus a large oligomeric species above 100 kDa (Fig. 8 *b*, lane 1). There was very little dimer species detected in the blot. Incubating Aβ40 with 1 mM SDS alters the oligomeric pattern, with the predominant species corresponding to monomeric Aβ and some dimer also present. The Aβ42-plus-1 mM SDS reaction also generated monomer and small oligomers, but there was an increase in the large oligomeric species above 100 kDa. In the presence of $Cu^{2+}$, bands corresponding to trimer were observed with Aβ40 (Fig. 8, lane 3). Incubating Aβ42 in the presence of $Cu^{2+}$ (Fig. 8, lane 3) showed a smaller band in the high molecular-weight range than that without $Cu^{2+}$ in 1 mM SDS, corresponding to the decrease in the 70 kDa peak in the size-exclusion chromatography. In micellar SDS (3 mM, 8 mM), only monomer and dimer bands were present on the Aβ40 gel (Fig. 8, lanes 5 and 6). The Aβ42-plus-micellar SDS reduced the amount of higher order oligomers and this was most pronounced at the highest SDS concentration used (8 mM).

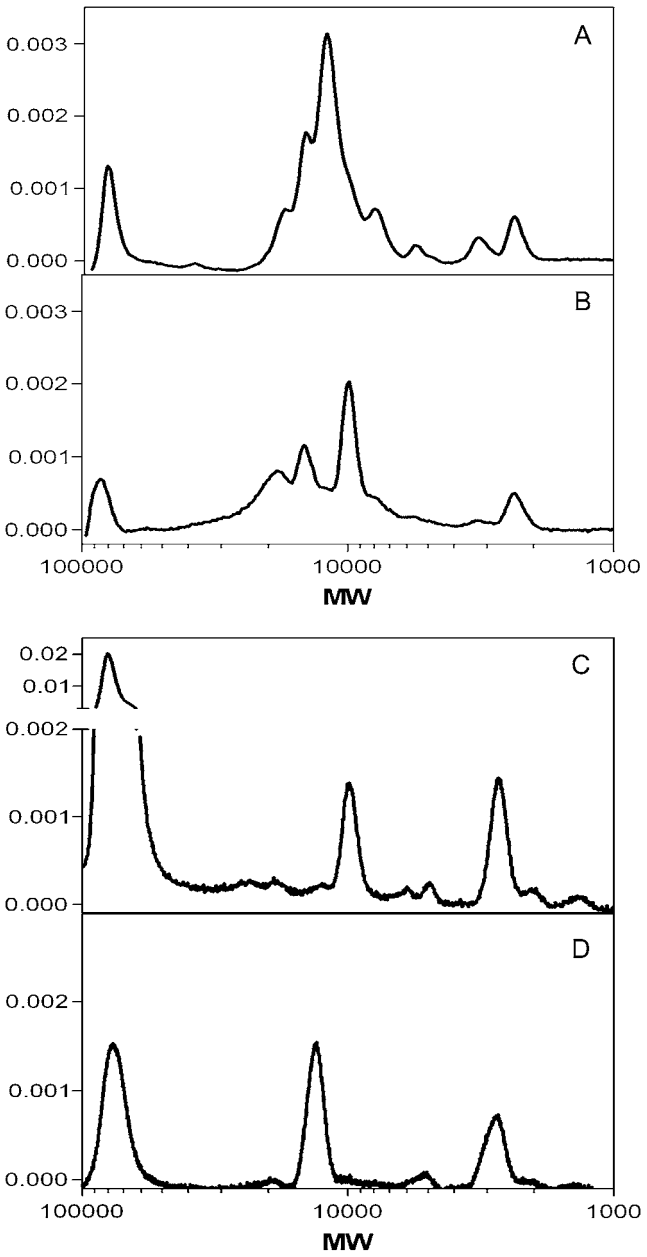


FIGURE 7 Size-exclusion chromatography. (*A*) A$\beta$40 in 1 mM SDS after overnight incubation at 37°C with stirring; (*B*) A$\beta$40 in 1 mM SDS and equimolar $Cu^{2+}$, after overnight incubation at 37°C with stirring; (*C*) A$\beta$42 in 1 mM SDS after overnight incubation at 37°C with stirring; and (*D*) A$\beta$42 in 1 mM SDS and equimolar $Cu^{2+}$, after overnight incubation at 37°C with stirring.

## Neuronal cell culture

### *A$\beta$40 and A$\beta$42 $\beta$-sheet conformations are toxic*

The toxic effect of A$\beta$ peptides has been associated with structural transitions to small oligomers, some of which have increased $\beta$-sheet conformation (42). To ascertain whether the submicellar SDS-induced changes in A$\beta$ conformation resulted in altered toxic properties, the viability of cortical neuronal cell culture in the presence of A$\beta$ in submicellar SDS solutions was determined. The effect of SDS on the cells was tested first, and when the final SDS concentration was $\leq$0.2 mM, there was no effect on cell viability (see Supplementary Material, Fig. S4).

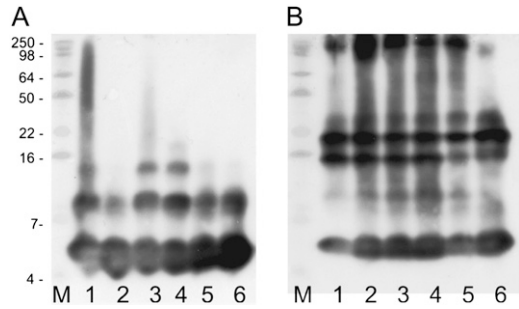


FIGURE 8 SDS-PAGE. (*A*) A$\beta$40 and (*B*) A$\beta$42, both gels loaded with A$\beta$ incubated overnight at 37°C with shaking. Lane *M* contains molecular-weight markers. Lane 1, A$\beta$; lane 2, A$\beta$ in 1 mM SDS; lane 3, A$\beta$ in 1 mM SDS + $Cu^{2+}$; lane 4, A$\beta$ in 1 mM SDS + $Zn^{2+}$; lane 5, A$\beta$ in 3 mM SDS; and lane 6, A$\beta$ in 8 mM SDS. The resolving matrix was a 16% Tris-Glycine SDS gel and the membrane probed with the monoclonal antibody WO2 (59).

In the absence of SDS, 10 $\mu$M A$\beta$40 was nontoxic to the neuronal cell cultures. However, in the presence of SDS, the A$\beta$40 had a toxic effect on cell viability that was dose-dependent for SDS—indicating that the $\beta$-sheet oligomers of A$\beta$40, induced by the presence of submicellar SDS, were toxic (Fig. 9 *b*). The toxic effect of the A$\beta$42 in the presence of SDS was also shown to be dose-dependent for SDS (Fig. 9 *b*). To determine whether the effects of SDS were specific for A$\beta$ peptide, non-A$\beta$ peptide neurotoxic agents, $H_2O_2$, and staurosporine (a broad spectrin kinase inhibitor), were examined in the presence of SDS. The addition of SDS had no effect on the amount of toxicity for either $H_2O_2$ or staurosporine at the different concentrations tested. These experiments confirm that the SDS effect was specific for A$\beta$ peptide (Fig. 9 *a*). When the A$\beta$ peptides were preincubated in SDS and equimolar copper, they were both shown to be toxic to neuronal cells (Fig. 9 *c*).

## DISCUSSION

In recent work, A$\beta$40 was studied in the presence of micellar SDS (43). The authors concluded that the increased rate of aggregation observed in the presence of SDS micelles was a result of the effective increase in concentration of A$\beta$ in the two-dimensional space on the surface of the micelles. In contrast, our work demonstrates the formation of stable, soluble $\beta$-sheet-rich oligomers of both A$\beta$40 and A$\beta$42 at much lower peptide concentrations (10 $\mu$M) in solutions containing submicellar SDS. The increased aggregation we observe is driven by structural transitions rather than effective increases in the local concentration of the peptide which has not been previously demonstrated to our knowledge.

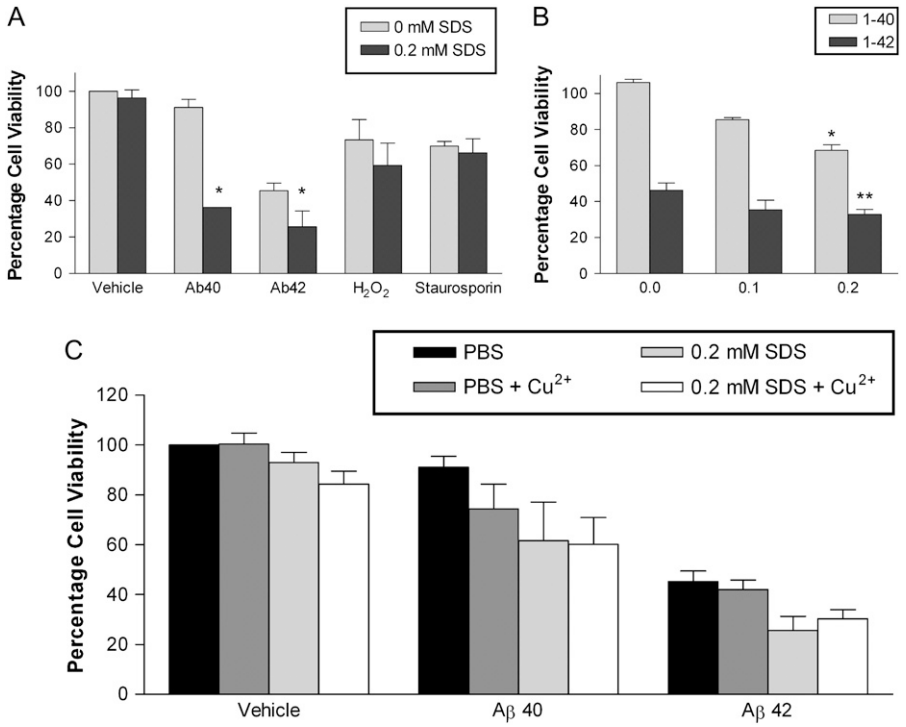


FIGURE 9 Toxicity assay. (*A*) The percentage cell survival of neuronal cells in the presence of A$\beta$40, A$\beta$42, $H_2O_2$, and staurosporine in neurobasal medium (*light-shaded representation*) and neurobasal medium containing 0.2 mM SDS (*light-shaded representation*). (*B*) The percentage cell survival of neuronal cells in the presence of A$\beta$40 (*light-shaded representation*) and A$\beta$42 (*medium-shaded representation*) in the presence of increasing concentration of SDS. (*C*) The percentage cell survival of neuronal cells in neurobasal medium, showing the toxicity of A$\beta$40 and A$\beta$42 in culture medium to which PBS (*solid representation*), PBS + $Cu^{2+}$ (*medium-shaded representation*), 0.2 mM SDS (*light-shaded representation*), or 0.2 mM SDS + $Cu^{2+}$ (*open representation*) has been added. Results are normalized and the data expressed as a percentage of the vehicle controls. Experiments are done in triplicate and results are expressed as mean $\pm$ SE. $N = 3$–7 for different treatment groups. Statistical comparisons between PBS alone and the different treatment groups were performed using Student's *t*-test. Asterisk indicates $p < 0.05$.

These oligomers were formed in the absence of metal ions, using chelex-treated buffers, conditions in which A$\beta$40 and A$\beta$42 are normally stable in solution (44). This work has also correlated the formation of stable soluble oligomers of both A$\beta$40 and A$\beta$42 with an increase in the toxicity of the peptides in neuronal cell culture.

While SDS is not a physiological substance, Barghorn et al. (25) have raised antibodies against oligomers generated by treating A$\beta$42 with submicellar SDS. These antibodies demonstrated cross-reactivity with brain tissue from AD patients and transgenic mice. These SDS-A$\beta$ oligomers were able to bind to the dendritic processes of neurons but not glia in hippocampal cell cultures and could block long-term potentiation in rat hippocampal slices. In the present work we have shown that the soluble oligomers of A$\beta$40 and A$\beta$42, prepared in submicellar SDS, showed a dose-dependent increase in toxicity. The conformation-activity relationship induced by the SDS is not known and therefore our biophysical studies have provided important molecular insights and indicate that, in the presence of submicellar SDS, both A$\beta$40 and 42 generate an interconverting ensemble of soluble $\beta$-sheet oligomers (Figs. 1 and 2).

We began by investigating the effect of the SDS concentration on the conformation of different length A$\beta$ peptides. The shorter A$\beta$ peptides, A$\beta$16 and A$\beta$28, which correspond to the extracellular N-terminal region of the peptide, are not toxic to cultured neuronal cells (45,46). A$\beta$16 is natively unstructured in aqueous solution and the titration of SDS caused no change in secondary conformation (Fig. 1), which indicates that it is the hydrophobic C-terminal domain of the longer peptides that drives the secondary structure transitions in A$\beta$. When SDS was titrated into a solution of A$\beta$28, there was an increase in $\alpha$-helical content at SDS concentrations above the CMC, consistent with previous results (39,40). While no $\beta$-sheet structure was detected at submicellar SDS concentrations, neither was an isodichroic point observed—indicating that the structural transition did not occur as a single transition. One interpretation of this result is that at submicellar concentrations of SDS, A$\beta$28 transiently inhabits $\beta$-sheet conformations. A$\beta$40 and A$\beta$42 are predominantly in an $\alpha$-helical conformation in micellar SDS as previously reported (39,40); however, at submicellar concentrations of SDS, both peptides were predominantly in a $\beta$-sheet conformation (Fig. 1).

The reversibility of the observed structural transitions was established by titrating $\alpha$-cyclodextrin, which can bind SDS and strip it from proteins (27), into the SDS/A$\beta$ solutions. Titration of $\alpha$-cyclodextrin into micellar SDS solutions of A$\beta$40 showed the structural transition from $\alpha$-helical to intermediate $\beta$-sheet conformation to be reversible, whereas the transition from $\beta$-sheet to random coil was not. Therefore, the folding and unfolding of A$\beta$ most likely occurs via different pathways or becomes trapped in a misfolded state (Fig. 2). The folding of A$\beta$ in SDS is not a reversible process at a given SDS concentration in either the folding or unfolding transition regions (47). The hysteresis observed in the chemical unfolding was mirrored in the thermal unfolding (Fig. 3) and indicates that there are tertiary or quaternary contacts involved. Both inter- and intraoligomeric contacts, which must be broken before unfolding can occur, delay

initial unfolding but are not reformed on folding. The differences between folding and unfolding were more marked in A$\beta$42.

While the exact mechanism of ThT binding to fibrils to cause increased fluorescence is unknown, recent work by Khurana et al. (48) has shown that ThT forms micelles at concentrations commonly used to study fibril growth by fluorescence assay (10–20 $\mu$M), which have a CMC of ~4 $\mu$M. Their data suggest that the positive charge on the ThT, combined with a nonpolar region, aid in the formation of ThT micelles and that the positive charges are then involved in binding in the grooves between the protofibrils of amyloid fibrils, enhancing the fluorescence of the ThT (48). Not all $\beta$-sheet structures are ThT-active.

Since the percentage of $\beta$-sheet content increased in the presence of SDS and A$\beta$ is known to form amyloidogenic structures, ThT fluorescence was used in conjunction with overnight incubations at 37°C to monitor any increase in ThT-active $\beta$-sheet content in the peptide solution. In the timeframe of this experiment, A$\beta$40 and A$\beta$42 did not form ThT-active aggregates in the absence of SDS or in the presence of micellar SDS. However, in the presence of submicellar SDS, ThT-positive structures were rapidly induced. ThT binds in the hydrophobic-tail region of the peptide, which becomes $\beta$-sheet in low SDS concentrations.

$^1$H NMR spectra of the A$\beta$ peptides in submicellar SDS were very broad, indicating that the amyloidogenic $\beta$-sheet structures were either very large and/or were in a dynamic equilibrium between different conformers such that the rate of exchange between the conformers was in the intermediate timeframe (~$\mu$M) of the NMR experiment. The presence of several different-sized species was confirmed by size-exclusion chromatography and SDS-PAGE analysis.

Without prior aging of the peptide in solution we have found that A$\beta$40 is reproducibly nontoxic to neuronal cell cultures. However, when incubated in submicellar SDS, to generate an interconverting ensemble of $\beta$-sheet oligomeric forms, the A$\beta$40 was toxic. The induction of toxicity in the normally nontoxic A$\beta$40 suggests that the toxicity is conformation-dependent rather than sequence-dependent, and is consistent with the notion that soluble $\beta$-sheet-rich oligomers of A$\beta$ represent the toxic species (10,49).

Although A$\beta$42 is the predominant alloform present in senile plaques, the level of A$\beta$42 has also been observed to increase in the normal aging brain, present in diffuse cortical plaques. However, a disease-specific increase in the relative level of A$\beta$40 in the brains of AD patients has been reported, suggesting that a substantial increase in A$\beta$40 may be detrimental to normal neuronal function, precipitating oligomerization and toxicity (50). Thus, the toxicity data presented for the A$\beta$40 peptide is particularly significant.

The biophysical data shows that A$\beta$42 more readily forms $\beta$-sheet structures and that once formed, these structures are more stable (Figs. 1 and 3, Table 3), consistent with the increased toxicity demonstrated by this peptide.

A$\beta$ interactions with metal ions are believed to be important in the development of AD (26,51). Transition metals such as copper, iron, and zinc are present in A$\beta$ plaques and have been implicated as a significant pathological risk factor in AD (52). In vivo, amyloid plaques taken from AD-affected brains are enriched in copper (~400 $\mu$M), zinc (~1 mM), and iron (~1 mM) (53–55). The solubilization of A$\beta$ from post-mortem brain tissue of AD patients is increased in the presence of metal chelators such as *n*,*n*,*n*′,*n*′-tetrakis(2-pyridyl-methyl)-ethylene-diamine and bathocuporine (56). Indeed, the use of the prototypic metal protein attenuating compounds such as clioquinol, a moderate metal chelator capable of inhibiting A$\beta$/Cu interactions, has shown promise as a therapeutic agent in both animal (57) and human clinical studies (58). A$\beta$ in the presence of copper has been demonstrated to be toxic to primary cortical neurones (59,60) and a potent inhibitor of the mitochondrial electron transport-chain complex cytochrome *c* oxidase (also known as complex IV) (61).

An emerging paradigm linking a number of degenerative diseases states that normal transient intermediate conformations of the causative protein agent accumulate and aggregate to form soluble $\beta$-sheet-rich oligomers and these soluble oligomers are the toxic agents (23). With regard to AD, soluble oligomers of A$\beta$ have been isolated from brain tissue (22) and correlate with the severity of neurodegeneration in AD (10).

## CONCLUSION

Previously the ability to study the structural transitions associated with the formation of $\beta$-sheet oligomeric structures has been hampered by the lack in solubility of the oligomeric species. In this study, we have been able to generate stable soluble oligomeric forms of A$\beta$ using submicellar concentrations of SDS, and this oligomerization has been driven by structural transitions in both A$\beta$40 and A$\beta$42 at low, physiologically relevant concentrations (56).

A range of biophysical data presented here indicates that the presence of $Cu^{2+}$ significantly shifts the A$\beta$ monomer-oligomer equilibrium, such that the formation and stability of soluble oligomeric $\beta$-sheet species is promoted by the presence of $Cu^{2+}$ and these soluble oligomeric forms of A$\beta$ are toxic to neuronal cells.

## SUPPLEMENTARY MATERIAL

To view all of the supplemental files associated with this article, visit www.biophysj.org.

Synchrotron radiation circular-dichroism was carried out with the support of the Daresbury Synchrotron Radiation Source and the assistance of David Clarke. We thank Timothy Johanssen for assistance with the cell-viability assays.

This work was funded by the National Health and Medical Research Council of Australia. D.P.S. is a Wellcome Traveling Fellow. Travel was

funded by the Australian Nuclear Science and Technology Organization through the Access to Major Resource Facilities Program.

## REFERENCES


1. Masters, C. L., G. Simms, N. A. Weinman, G. Multhaup, B. L. McDonald, and K. Beyreuther. 1985. Amyloid plaque core protein in Alzheimer disease and Down syndrome. *Proc. Natl. Acad. Sci. USA.* 82:4245–4249.
2. Masters, C. L., R. Cappai, K. J. Barnham, and V. L. Villemagne. 2006. Molecular mechanisms for Alzheimer's disease: implications for neuroimaging and therapeutics. *J. Neurochem.* 97:1700–1725.
3. Geula, C., C. K. Wu, D. Saroff, A. Lorenzo, M. Yuan, and B. A. Yankner. 1998. Aging renders the brain vulnerable to amyloid [β]-protein neurotoxicity. *Nat. Med.* 4:827–831.
4. Yankner, B. A., L. K. Duffy, and D. A. Kirschner. 1990. Neurotrophic and neurotoxic effects of amyloidβ protein: reversal by tachykinin neuropeptides. *Science.* 250:279–282.
5. Hendriks, L., C. M. van Duijn, P. Cras, M. Cruts, W. Van Hul, F. van Harskamp, A. Warren, M. G. McInnis, S. E. Antonarakis, and A. Martin. 1992. Presenile dementia and cerebral hemorrhage linked to a mutation at codon 692 of the β-amyloid precursor protein gene. *Nat. Genet.* 1:218–221.
6. Levy, E., M. D. Carman, I. J. Fernandez-Madrid, M. D. Power, I. Lieberburg, S. G. Van Duinen, G. T. A. M. Bots, W. Luyendijk, and B. Frangione. 1990. Mutation of the Alzheimer's disease amyloid gene in hereditary cerebral hemorrhage, Dutch type. *Science.* 248:1124–1126.
7. Miravalle, L., T. Tokuda, R. Chiarle, G. Giaccone, O. Bugiani, F. Tagliavini, B. Frangione, and J. Ghiso. 2000. Substitutions at codon 22 of Alzheimer's Aβ peptide induce diverse conformational changes and apoptotic effects in human cerebral endothelial cells. *J. Biol. Chem.* 275:27110–27116.
8. Nilsberth, C., A. Westlind-Danielsson, C. B. Eckman, M. M. Condron, K. Axelman, C. Forsell, C. Stenh, J. Luthman, D. B. Teplow, and A. Younkin. 2001. The ''Arctic'' APP mutation (E693G) causes Alzheimer's disease by enhanced Aβ protofibril formation. *Nat. Neurosci.* 4:887–893.
9. Grabowski, T. J., H. S. Cho, J. P. Vonsattel, G. W. Rebeck, and S. M. Greenberg. 2001. Novel amyloid precursor protein mutation in an Iowa family with dementia and severe cerebral amyloid angiopathy. *Ann. Neurol.* 49:697–705.
10. McLean, C. A., R. A. Cherny, F. W. Fraser, S. J. Fuller, M. J. Smith, K. V. Beyreuther, A. I. Bush, and C. L. Masters. 1999. Soluble pool of Aβ amyloid as a determinant of severity of neurodegeneration in Alzheimer's disease. *Ann. Neurol.* 46:860–866.
11. Cummings, B. J., C. J. Pike, R. Shankle, and C. W. Cotman. 1996. β-amyloid deposition and other measures of neuropathology predict cognitive status in Alzheimer's disease. *Neurobiol. Aging.* 17:921–933.
12. Berg, L., D. W. McKeel, Jr., J. P. Miller, M. Storandt, E. H. Rubin, J. C. Morris, J. Baty, M. Coats, J. Norton, A. M. Goate, J. L. Price, M. Gearing, S. S. Mirra, and A. M. Saunders. 1998. Clinicopathologic studies in cognitively healthy aging and Alzheimer's disease: relation of histologic markers to dementia severity, age, sex, and apolipoprotein-E genotype. *Arch. Neurol.* 55:326–335.
13. Lesne, S., M. T. Koh, L. Kotilinek, R. Kayed, C. G. Glabe, A. Yang, M. Gallagher, and K. H. Ashe. 2006. A specific amyloid-β protein assembly in the brain impairs memory. *Nature.* 440:352–357.
14. Bitan, G., M. D. Kirkitadze, A. Lomakin, S. S. Vollers, G. B. Benedek, and D. B. Teplow. 2003. Amyloid β-protein (Aβ) assembly: Aβ 40 and Aβ 42 oligomerize through distinct pathways. *Proc. Natl. Acad. Sci. USA.* 100:330–335.
15. Harper, J. D., S. S. Wong, C. M. Lieber, and P. T. Lansbury. 1997. Observation of metastable Aβ amyloid protofibrils by atomic force microscopy. *Chem. Biol.* 4:119–125.
16. Lambert, M. P., A. K. Barlow, B. A. Chromy, C. Edwards, R. Freed, M. Liosatos, T. E. Morgan, I. Rozovsky, B. Trommer, K. L. Viola, P. Wals, C. Zhang, C. E. Finch, G. A. Krafft, and W. L. Klein. 1998. Diffusible, nonfibrillar ligands derived from Aβ 1–42 are potent central nervous system neurotoxins. *Proc. Natl. Acad. Sci. USA.* 95:6448–6453.
17. Oda, T., P. Wals, H. H. Osterburg, S. A. Johnson, G. M. Pasinetti, T. E. Morgan, I. Rozovsky, W. B. Stine, S. W. Snyder, T. F. Holzman, G. A. Krafft, and C. E. Finch. 1995. Clusterin (apoJ) alters the aggregation of amyloid β-peptide (Aβ 1–42) and forms slowly sedimenting Aβ complexes that cause oxidative stress. *Exp. Neurol.* 136:22–31.
18. Sun, X. D., Z. L. Mo, B. M. Taylor, and D. E. Epps. 2003. A slowly formed transient conformer of Aβ (1-40) is toxic to inward channels of dissociated hippocampal and cortical neurons of rats. *Neurobiol. Dis.* 14:567–578.
19. Taylor, B. M., R. W. Sarver, G. Fici, R. A. Poorman, B. S. Lutzke, A. Molinari, T. Kawabe, K. Kappenman, A. E. Buhl, and D. E. Epps. 2003. Spontaneous aggregation and cytotoxicity of the β-amyloid Aβ1-40: a kinetic model. *J. Protein Chem.* 22:31–40.
20. Walsh, D. M., A. Lomakin, G. B. Benedek, M. M. Condron, and D. B. Teplow. 1997. Amyloid β-protein fibrillogenesis. Detection of a protofibrillar intermediate. *J. Biol. Chem.* 272:22364–22372.
21. Dahlgren, K. N., A. M. Manelli, W. B. Stine, Jr., L. K. Baker, G. A. Krafft, and M. J. LaDu. 2002. Oligomeric and fibrillar species of amyloid-β peptides differentially affect neuronal viability. *J. Biol. Chem.* 277:32046–32053.
22. Kuo, Y.-M., M. R. Emmerling, C. Vigo-Pelfrey, T. C. Kasunic, J. B. Kirkpatrick, G. H. Murdoch, M. J. Ball, and A. E. Roher. 1996. Water-soluble Aβ (N-40, N-42) oligomers in normal and Alzheimer disease brains. *J. Biol. Chem.* 271:4077–4081.
23. Kayed, R., E. Head, J. L. Thompson, T. M. McIntire, S. C. Milton, C. W. Cotman, and C. G. Glabe. 2003. Common structure of soluble amyloid oligomers implies common mechanism of pathogenesis. *Science.* 300:486–489.
24. Terry, R. 1999. The neuropathology of Alzheimer disease and the structural basis of its cognitive alterations. *In* Alzheimer Disease. R. D. Terry, editor. Lippincott, Williams and Wilkins, Philadelphia, PA.
25. Barghorn, S., V. Nimmrich, A. Striebinger, C. Krantz, P. Keller, B. Janson, M. Bahr, M. Schmidt, R. S. Bitner, J. Harlan, E. Barlow, U. Ebert, and H. Hillen. 2005. Globular amyloid β-peptide oligomer—a homogenous and stable neuropathological protein in Alzheimer's disease. *J. Neurochem.* 95:834–847.
26. Bush, A. I. 2003. The metallobiology of Alzheimer's disease. *Trends Neurosci.* 26:207–214.
27. Otzen, D. E., and M. Oliveberg. 2001. A simple way to measure protein refolding rates in water. *J. Mol. Biol.* 313:479–483.
28. Hingerty, B., B. Klar, G. L. Hardgrove, C. Betzel, and W. Saenger. 1984. Neutron diffraction of α, β and γ cyclodextrins: hydrogen bonding patterns. *J. Biomol. Struct. Dyn.* 2:249–260.
29. Nath, U., and J. B. Udgaonkar. 1995. Perturbation of a tertiary hydrogen bond in barstar by mutagenesis of the sole His residue to Gln leads to accumulation of at least one equilibrium folding intermediate. *Biochemistry.* 34:1702–1713.
30. Whitmore, L., and B. A. Wallace. 2004. DICHROWEB, an online server for protein secondary structure analyses from circular dichroism spectroscopic data. *Nucleic Acids Res.* 32:W668–W673.
31. Lobley, A., L. Whitmore, and B. A. Wallace. 2002. DICHROWEB: an interactive website for the analysis of protein secondary structure from circular dichroism spectra. *Bioinformatics.* 18:211–212.
32. Provencher, S. W., and J. Glockner. 1981. Estimation of globular protein secondary structure from circular dichroism. *Biochemistry.* 20: 33–37.
33. Barnham, K. J., G. D. Ciccotosto, A. K. Tickler, F. E. Ali, D. G. Smith, N. A. Williamson, Y. H. Lam, D. Carrington, D. Tew, G. Kocak, I. Volitakis, F. Separovic, C. J. Barrow, J. D. Wade, C. L. Masters, R. A. Cherny, C. C. Curtain, A. I. Bush, and R. Cappai. 2003. Neurotoxic, redox-competent Alzheimer's β-amyloid is released from lipid membrane by methionine oxidation. *J. Biol. Chem.* 278:42959–42965.

34. Ida, N., T. Hartmann, J. Pantel, J. Schroder, R. Zerfass, H. Forstl, R. Sandbrink, C. L. Masters, and K. Beyreuther. 1996. Analysis of heterogeneous A4 peptides in human cerebrospinal fluid and blood by a newly developed sensitive Western blot assay. *J. Biol. Chem.* 271:22908–22914.

35. Santoro, M. M., and D. W. Bolen. 1988. Unfolding free energy changes determined by the linear extrapolation method. 1. Unfolding of phenylmethanesulfonyl $\alpha$-chymotrypsin using different denaturants. *Biochemistry.* 27:8063–8068.

36. Bartels, C., T. H. Xia, M. Billeter, P. Guntert, and K. Wuthrich. 1995. The program XEASY for computer-supported NMR spectral-analysis of biological macromolecules. *J. Biomol. NMR.* 6:1–10.

37. Fuguet, E., C. Rafols, M. Roses, and E. Bosch. 2005. Critical micelle concentration of surfactants in aqueous buffered and unbuffered systems. *Anal. Chim. Acta.* 548:95–100.

38. Corrin, M. L., and W. D. Harkins. 1947. The effect of salts on the critical concentration for the formation of micelles in colloidal electrolytes. *J. Am. Chem. Soc.* 69:683–688.

39. Shao, H., S. Jao, K. Ma, and M. G. Zagorski. 1999. Solution structures of micelle-bound amyloid $\beta$-(1-40) and $\beta$-(1-42) peptides of Alzheimer's disease. *J. Mol. Biol.* 285:755–773.

40. Coles, M., W. Bicknell, A. A. Watson, D. P. Fairlie, and D. J. Craik. 1998. Solution structure of amyloid $\beta$-peptide(1-40) in a water-micelle environment. Is the membrane-spanning domain where we think it is? *Biochemistry.* 37:11064–11077.

41. Zagorski, M. G., and C. J. Barrow. 1992. NMR studies of amyloid $\beta$-peptides: proton assignments, secondary structure, and mechanism of an $\alpha$-helix$\rightarrow\beta$-sheet conversion for a homologous, 28-residue, N-terminal fragment. *Biochemistry.* 31:5621–5631.

42. Huang, T. H., D. S. Yang, N. P. Plaskos, S. Go, C. M. Yip, P. E. Fraser, and A. Chakrabartty. 2000. Structural studies of soluble oligomers of the Alzheimer $\beta$-amyloid peptide. *J. Mol. Biol.* 297:73–87.

43. Rangachari, V., D. K. Reed, B. D. Moore, and T. L. Rosenberry. 2006. Secondary structure and interfacial aggregation of amyloid-$\beta$ (1-40) on sodium dodecyl sulfate micelles. *Biochemistry.* 45:8639–8648.

44. Huang, X., C. S. Atwood, R. D. Moir, M. A. Hartshorn, R. E. Tanzi, and A. I. Bush. 2004. Trace metal contamination initiates the apparent auto-aggregation, amyloidosis, and oligomerization of Alzheimer's A$\beta$ peptides. *J. Biol. Inorg. Chem.* 9:954–960.

45. Thompson, A., A. R. White, C. McLean, C. L. Masters, R. Cappai, and C. J. Barrow. 2000. Amyloidogenicity and neurotoxicity of peptides corresponding to the helical regions of $PrP_C$. *J. Neurosci. Res.* 62: 293–301.

46. Liu, R., C. McAllister, Y. Lyubchenko, and M. R. Sierks. 2004. Residues 17–20 and 30–35 of $\beta$-amyloid play critical roles in aggregation. *J. Neurosci. Res.* 75:162–171.

47. Pace, C. N., and D. V. Laurents. 1989. A new method for determining the heat capacity change for protein folding. *Biochemistry.* 28:2520–2525.

48. Khurana, R., C. Coleman, C. Ionescu-Zanetti, S. A. Carter, V. Krishna, R. K. Grover, R. Roy, and S. Singh. 2005. Mechanism of Thioflavin-T binding to amyloid fibrils. *J. Struct. Biol.* 151:229–238.

49. Hartley, D. M., D. M. Walsh, C. P. Ye, T. Diehl, S. Vasquez, P. M. Vassilev, D. B. Teplow, and D. J. Selkoe. 1999. Protofibrillar intermediates of amyloid $\beta$-protein induce acute electrophysiological changes and progressive neurotoxicity in cortical neurons. *J. Neurosci.* 19:8876–8884.

50. Gregory, G. C., and G. M. Halliday. 2005. What is the dominant A$\beta$ species in human brain tissue? A review. *Neurotox. Res.* 7:29–41.

51. Barnham, K. J., F. Haeffner, G. D. Ciccotosto, C. C. Curtain, D. Tew, C. Mavros, K. Beyreuther, D. Carrington, C. L. Masters, R. A. Cherny, R. Cappai, and A. I. Bush. 2004. Tyrosine gated electron transfer is key to the toxic mechanism of Alzheimer's disease $\beta$-amyloid. *FASEB J.* 18:1427–1429.

52. Bush, A. I. 2000. Metals and neuroscience. *Curr. Opin. Chem. Biol.* 4:184–191.

53. Lovell, M. A., J. D. Robertson, W. J. Teesdale, J. L. Campbell, and W. R. Markesbery. 1998. Copper, iron and zinc in Alzheimer's disease senile plaques. *J. Neurol. Sci.* 158:47–52.

54. Lee, J.-Y., I. Mook-Jung, and J.-Y. Koh. 1999. Histochemically reactive zinc in plaques of the Swedish mutant $\beta$-amyloid precursor protein transgenic mice. *J. Neurosci.* 19:1–5.

55. Suh, S. W., K. B. Jensen, M. S. Jensen, D. S. Silva, P. J. Kesslak, G. Danscher, and C. J. Frederickson. 2000. Histochemically reactive zinc in amyloid plaques, angiopathy, and degenerating neurons of Alzheimer's diseased brains. *Brain Res.* 852:274–278.

56. Cherny, R. A., J. T. Legg, C. A. McLean, D. P. Fairlie, X. Huang, C. S. Atwood, K. Beyreuther, R. E. Tanzi, C. L. Masters, and A. I. Bush. 1999. Aqueous dissolution of Alzheimer's disease A$\beta$ amyloid deposits by biometal depletion. *J. Biol. Chem.* 274:23223–23228.

57. Cherny, R. A., C. S. Atwood, M. E. Xilinas, D. N. Gray, W. D. Jones, C. A. McLean, K. J. Barnham, I. Volitakis, F. W. Fraser, Y. Kim, X. Huang, L. E. Goldstein, R. D. Moir, J. T. Lim, K. Beyreuther, H. Zheng, R. E. Tanzi, C. L. Masters, and A. I. Bush. 2001. Treatment with a copper-zinc chelator markedly and rapidly inhibits $\beta$-amyloid accumulation in Alzheimer's disease transgenic mice. *Neuron.* 30:665–676.

58. Ritchie, C. W., A. I. Bush, A. Mackinnon, S. Macfarlane, M. Mastwyk, L. MacGregor, L. Kiers, R. Cherny, Q. X. Li, A. Tammer, D. Carrington, C. Mavros, I. Volitakis, M. Xilinas, D. Ames, S. Davis, K. Beyreuther, R. E. Tanzi, and C. L. Masters. 2003. Metal-protein attenuation with iodochlorhydroxyquin (clioquinol) targeting A$\beta$ amyloid deposition and toxicity in Alzheimer disease: a pilot phase-2 clinical trial. *Arch. Neurol.* 60:1685–1691.

59. Cuajungco, M. P., L. E. Goldstein, A. Nunomura, M. A. Smith, J. T. Lim, C. S. Atwood, X. Huang, Y. W. Farrag, G. Perry, and A. I. Bush. 2000. Evidence that the $\beta$-amyloid plaques of Alzheimer's disease represent the redox-silencing and entombment of A$\beta$ by zinc. *J. Biol. Chem.* 275:19439–19442.

60. Huang, X., C. S. Atwood, M. A. Hartshorn, G. Multhaup, L. E. Goldstein, R. C. Scarpa, M. P. Cuajungco, D. N. Gray, J. Lim, R. D. Moir, R. E. Tanzi, and A. I. Bush. 1999. The A$\beta$ peptide of Alzheimer's disease directly produces hydrogen peroxide through metal ion reduction. *Biochemistry.* 38:7609–7616.

61. Crouch, P. J., R. Blake, J. A. Duce, G. D. Ciccotosto, Q. X. Li, K. J. Barnham, C. C. Curtain, R. A. Cherny, R. Cappai, T. Dyrks, C. L. Masters, and I. A. Trounce. 2005. Copper-dependent inhibition of human cytochrome *c* oxidase by a dimeric conformer of amyloid $\beta$1-42. *J. Neurosci.* 25:672–679.